Molecular Crystals and Liquid Crystals
Publication details, including instructions for authors and subscription information:
http://www.tandfonline.com/loi/gmcl18

Polymer-Dispersed Liquid Crystal Films Formed By Electron-Beam Cure

Nuno A. Vaz [a] , George W. Smith [a] & G. Paul Montgomery Jr. [a]
[a] Physics Department, General Motors Research Laboratories, Warren, MI, 48090-9055

Version of record first published: 24 Sep 2006.

To cite this article: Nuno A. Vaz , George W. Smith & G. Paul Montgomery Jr. (1991): Polymer-Dispersed Liquid Crystal Films Formed By Electron-Beam Cure, Molecular Crystals and Liquid Crystals, 197:1, 83-101

To link to this article: http://dx.doi.org/10.1080/00268949108029704

Mol. Cryst. Liq. Cryst., 1991, Vol. 197, pp. 83–101
Reprints available directly from the publisher
Photocopying permitted by license only

Printed in the United States of America

Polymer-Dispersed Liquid Crystal Films Formed By Electron-Beam Cure

NUNO A. VAZ, GEORGE W. SMITH and G. PAUL MONTGOMERY, JR.
Physics Department, General Motors Research Laboratories, Warren, MI 48090-9055

(Received May 1990; in final form November 1990)

Polymer-dispersed liquid crystal (PDLC) films are useful in electro-optic applications because they can be switched electrically between opaque and transparent states. We have prepared PDLC films using electron-beam radiation (e-beam cure). The resulting films exhibit promising mechanical, electro-optic, and thermal response. Compared with the ultraviolet cure process, e-beam cure has the advantage of not requiring photoinitiators. In addition, e-beam cure is characterized by a fast cure rate. The e-beam cure method may, therefore, be a good candidate for production of PDLC films.

Keywords: polymer-dispersed liquid crystal, nematic, electron-beam, electro-optics

I. INTRODUCTION

Polymer-dispersed liquid crystal (PDLC) films are thin films composed of liquid crystalline micro-droplets dispersed in solid matrices.[1–3] These films are promising materials for light control and electro-optic applications because they can be switched electrically from a light scattering "off-state" to a highly transparent "on-state." They have been prepared by both phase separation processes[1–5] and a microencapsulation technique.[6,7] Phase separation has been produced by thermal cure of the polymer,[1,3,4] ultraviolet (UV) cure,[2] cooling a thermoplastic/liquid crystal mixture,[5] and evaporation of the solvent from a thermoplastic/liquid crystal/solvent mixture.[5]

Each of these preparation methods has its own advantages. The use of thermoplastics allows for the easy reprocessing of the polymer and liquid crystal materials after unsuccessful runs. Thermal polymerization was the first phase separation technique discovered and, therefore, expertise is greatest in this area; it has been used to prepare PDLC films with long term memory. Finally, the ultraviolet cure process leads to fast and very precise control of the polymer cure.

Each of those techniques also has its own drawbacks, some of which are indicated here:

1. The thermal cure of epoxies is extremely temperature-sensitive; cure begins immediately upon mixing of components and is relatively slow at room tem-

perature. Moreover, epoxy systems often show poor light stability because proper refractive index matching of the polymer matrix to the liquid crystal[8] requires the addition of less stable aromatic epoxides to light-stable aliphatic epoxides.

2. In the thermoplastic cooling method droplet size is determined by cooling rate which may be somewhat non-uniform or difficult to control. Thermoplastic solvent evaporation establishes the droplet size by the evaporation rate which may be slow and sensitive to temperature.[5,9] Solvent retention must be guarded against; solvent capture and elimination is a difficult technical problem with possible environmental considerations. Moreover, thermoplastics—which are essential in these two techniques—exhibit a more pronounced dependence of their refractive index on temperature than thermosets.[10] This may be responsible for a rapid variation of film transmittance with temperature.[8,10]
3. Ultraviolet cure requires the use of photoinitiators which, because they continuously absorb UV radiation and relax by exciting the surrounding molecules, may shorten film life or react with the dispersed liquid crystal material unless special protective steps are taken.[11]

We have prepared PDLC films using an electron-beam to cure the polymer matrix. In this paper we describe the films prepared using this process, discuss their structure as determined from scanning electron microscope (SEM) micrographs, present and interpret calorimetric data, discuss the electro-optic performance of the films, and, finally, discuss some of the benefits and limitations of using the e-beam technique to form PDLC films.

II. MATERIALS AND SAMPLE PREPARATION

A. Materials

A.1 Polymer Matrices. Polymer resins suitable for e-beam cure are basically the same as those used in free-radical UV-curing processes except that, clearly, no photoinitiator has to be added to the polymer resin.[12] The presence of a photoinitiator, however, does not interfere with the e-beam cure process. Thus, we have used both commercial UV-curable resins which incorporate a photoinitiator and e-beam formulations prepared in our laboratory without photoinitiators.

The e-beam cure time of polymer resins varies with the type of functional group.[13] The following list orders some functional groups according to increasing cure time:[13] *acrylates, methacrylates, vinyls, allyls.* In our study we used four formulations involving different types of functional groups:

1. NOA65A is a formulation based on the commercially available resin Norland Optical Adhesive NOA65.[14] This material has been widely used to prepare UV-cured PDLC films with good results.[2] It is a thiol-ene system (allyl system) with mercaptan derivatives and a benzophenone photoinitiator. To it we added 2% of a photoaccelerator[15] to produce the formulation NOA65A.

2. P5007P is an acrylate, mercaptan-activated formulation consisting of the diacrylate oligomer Photomer 5007[16] mixed with pentaerythritol tetraacrylate (PETA)[17] in the volume ratio 2:1.
3. P6008P is an acrylate formulation consisting of Photomer 6008[16] and PETA[17] in the volume ratio 2:1.
4. DUDMAP is an acrylate formulation consisting of a diurethane dimethacrylate[17] and PETA[17] in the volume ratio 2:1.

A.2 Liquid Crystals. We used three commercially available liquid crystal mixtures: E7,[18] E63,[18] and ROTN404.[19] E7 is a mixture of cyanobiphenyl and cyanoterphenyl liquid crystalline materials. E63 contains, in addition, cyanophenylcyclohexane derivatives and a cyanobiphenyl ester liquid crystal. Finally, ROTN404 contains cyanobiphenyls, one cyanoterphenyl and cyanophenylpyrimidines.

A.3 Substrates. Because energetic radiation is known to create color centers in many transparent materials, we evaluated several possible substrate materials. Since we were interested in evaluating electro-optical properties, we used transparent substrates with transparent conducting coatings: soda lime glass,[20] thin flexible glass,[21] and polyester (PET) coated with a transparent conducting layer of indium-tin oxide (ITO).[22] For completeness, we also tested polycarbonate (PC) and epoxy films (both unavailable with ITO coatings). The results show that, after an exposure to 25 Mrad, the substrates could be rated in order of increasing discoloration as: *PET, PC, glass, flexible glass, epoxy*. We note that the epoxy material showed a particularly strong discoloration. Since the polyester (PET) coated with a transparent conducting layer of indium-tin oxide (PET/ITO)[16] was the least discolored substrate, all the films described in this work used PET/ITO substrates.

B. Sample Preparation

Each sample consisted of a PDLC film cured between two PET/ITO substrates. A mixture containing the desired proportions of liquid crystal and polymer precursors was first prepared and spread between the PET/ITO substrates. It was then exposed to the e-beam radiation to cure the polymer by placing the assembly on a metal plate pre-heated to ~50°C on top of a conveyor belt running at 0.05 m/s (see Figure 1).

Glass microfiber spacers[23] were used to control film thickness; however, in our experiments it was difficult to press the two PET substrates against each other in

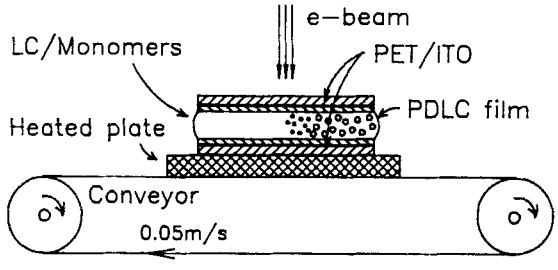

FIGURE 1 Schematic illustration of PDLC film cure by an e-beam.

TABLE I

Characterization of e-Beam-Cured Samples. (G = good, P = poor, F = failure, R = rigid, RM = reverse morphology)

Sample No.	Formulation[a]	Dose (Mrad)	L[b] (μm)	$\overline{D}$[c] (μm)	S-E[d]	E/O[e]	T/O[f]	E[g]
1	System 1 (1:1)	20	48	< 0.1	G	P	G	G
2	System 1 (1:0.75)	20	—	—	F	—	—	—
3	System 1 (1:1)	10	41	0.28	G	G	G	G
4	System 2 (1:1)	5	64	RM	G	P	G	R
5	System 2 (1:1)	10	77	RM	G	P	G	R
6	System 2 (1:1)	20	74	RM	G	P	P	R
7	System 3 (1:1)	6	—	RM	F	F	F	R
8	System 4 (1:1)	10	32	RM	G	F	G	R
9	System 4 (1:1)	20	—	RM	G	F	G	R

[a] System 1 = NOA65A/ROTN404; System 2 = P5007P/ROTN404; System 3 = PETA/ROTNH404; System 4 = DUDMAP/E63; the numbers in parentheses are the liquid crystal to polymer volume ratios.
[b] L = Sample thickness.
[c] $\overline{D}$ = Mean droplet diameter.
[d] S-E = Scattering efficiency.
[e] E/O = Electro-optic response.
[f] T/O = Thermo-optic response.
[g] E = Elongation under a linear applied stress.

the e-beam apparatus. Consequently, film thickness varied considerably, both within a single film and from film to film (see Table I). However, this is not an inherent problem which would make the use of PET or e-beam cure impractical.

III. ELECTRON-BEAM CURE TECHNIQUE

A. e-Beam Equipment

We used an Electrocurtain Model P250S e-beam machine[24] in which the e-beam is produced by a linear filament and accelerated with a bias voltage of up to 250 kV. The electrons traveling in the vacuum chamber are allowed to escape into air through a titanium foil window a few micrometers thick. In our experiment the sample was passed under the electron beam by placing it over a heated plate on a conveyor belt which ran at an adjustable speed. The sample was irradiated in air. The parameters which characterize the cure conditions are the line speed v, the filament current I, and the yield factor k. The line speed determines the exposure time of the product, the filament or beam current I determines the number of electrons per second received by the product (the energy delivery rate), and the yield factor k characterizes the processor's performance. These parameters are used to determine the dose, D, through the relation $D(\text{Mrad}) = kI(\text{mA})/v(\text{ft/min})$. In our experiments the e-beam machine was operated with a belt speed of 10 ft/min (0.05 m/s), a yield factor of 24, and current levels ranging from 2 to 10 mA,

giving doses in the range of 5 to 25 Mrad. Total exposure time was about 1 s. The 225 kV accelerating voltage in our experiments produced electrons with a penetration depth (half-dose thickness) of 230 μm in PET. Since our PET substrates were 178 μm thick, the e-beam dose should have been sufficient to cure our PDLC films.

Finally, the length and width of the electron beam were 0.4 m and 0.05 m, respectively. The width is important for estimating the temperature rise experienced by the sample during its exposure to the intense radiation (see below).

B. Cure Temperature

Due to the high energy level of the electrons bombarding the sample, we expected the temperature of the sample to rise during the exposure time. Since we have established in the past that the micro-structure and electro-optic behavior of PDLC films depend strongly on the cure conditions, including the cure temperature,[25-31] it was important to estimate the temperature rise of the sample due to the e-beam exposure.

From energy conservation we let:

$$D(x) = c\Delta T - \Delta H \tag{1}$$

where D is the dosage which is a function of the distance x measured from the top surface of the sample inwards, ΔT is the rise in temperature experienced by a material with specific heat c, and ΔH is the heat of polymerization. Taking the experimental values $D = 20$ Mrad $= 48$ cal g^{-1},[32] $c = 0.5$ cal g^{-1},[33] $\Delta H = 25$ cal g^{-1},[34,35] and an initial temperature of 50°C (established by the heated plate carrying the sample), we estimate the maximum cure temperature to be 90°C.

However, the cure temperature actually experienced by the sample may be less than 90°C due to diffusion of heat from the sample during the time the sample is under the e-beam. This time is easily computed from the belt speed of 0.05 m/s and the beam width of 0.05 m to be 1 s. Taking the thermal diffusivity, β, of the PET substrate[36,37] to be $\beta = 8 \times 10^{-2}$ mm^2 s^{-1}, and using the usual expression

$$l = \sqrt{2\beta t} \tag{2}$$

for the average distance l over which heat will diffuse in a time t, we estimate $l = 400$ μm during $t = 1$ s. Thus, some of the heat generated in the sample will diffuse out and the overall temperature rise of the sample will be less than 90°C. An independent assessment of the cure temperature from calorimetry will be discussed in *IV.A*. Suffice it to say that, from the calorimetric data, we estimate the cure temperature to be about 77°C.

IV. RESULTS

We will first present calorimetric results for two e-beam-cured samples: a PDLC film and a film containing only the polymer resin of that sample, NOA65A. Then we will discuss the microstructure and the electro-optic performance of all the

samples summarized in Table I. This table shows the composition of each sample, the thickness, L, of the PDLC film, the average liquid crystal microdroplet diameter, $\overline{D}$, and the sample's ratings in terms of its scattering efficiency and electro-optic response.

A. Calorimetry

The differential scanning calorimeter (DSC) used in these studies has been described previously.[1,2,25,26] Using the calorimeter in its scanning mode, we can determine first order phase transformation temperatures and enthalpies as well as glass transition temperatures of PDLC systems.

The nematic-isotropic transition temperature, T_{NI}, determines the maximum operating temperature of a PDLC film. Calorimetrically determined nematic-isotropic transition temperatures are generally close to those for the pure liquid crystal. However, the polymer matrix selected can shift T_{NI}, due either to preferential dissolution of liquid crystal components in the matrix or to residual polymer precursor remaining in the liquid crystal. The former effect generally yields higher values of T_{NI} since lighter, lower temperature components tend to remain in the matrix; the latter is an impurity effect which depresses T_{NI}. As a result, both decreases and increases in T_{NI} have been reported. The liquid crystal (ROTN-404) used in this work has a transition temperature of about 110°C in the pure state; however, in a PDLC film based on NOA65A (either e-beam or UV-cured), T_{NI} is depressed to about 100°C.[26–28] From the magnitude of the nematic-isotropic transition enthalpy, ΔH_{NI}, one can estimate the fraction of liquid crystal contained in the micro-droplets.[25]

The glass transition temperature, T_g, is of interest because it is a measure of the temperature below which the film loses its flexibility. Since T_g is a function of the cure temperature, the magnitude of T_g also provides information on T_{cure}. T_g is also affected by the amount of liquid crystal in the PDLC film. In general, an increase in liquid crystal concentration results in a reduction of T_g.

In the present work DSC scans also provided us with a means to ascertain whether a sample was fully cured by the e-beam. The presence of a high temperature exotherm indicated the occurrence of additional cross-linking (i.e., the sample was initially incompletely cured). Furthermore, an increase in T_g in DSC scans following an initial heat treatment suggested that the treatment resulted in a greater degree of cure.

A.1 Pure Polymer Matrix (NOA65A). Figure 2 shows two DSC scans of an e-beam-cured sample of pure polymer matrix, NOA65A. Figure 2a is the scan for the sample on the first heating cycle and Figure 2b is for subsequent scans. A comparison reveals two main differences: the high temperature exotherm of 2*a* is absent in 2*b*; and T_g has increased from 287 K (14°C) to 290 K (17°C) in going from 2*a* to 2*b*. As mentioned above, the exotherm indicates that thermal cure occurs when the as-received sample is initially heated to a sufficiently high temperature. Following this thermal cure, the sample is more fully cross-linked as revealed in Figure 2b by the absence of the exotherm and the higher value of T_g. If we assume that the dependence of T_g on T_{cure} for e-beam cured samples is similar

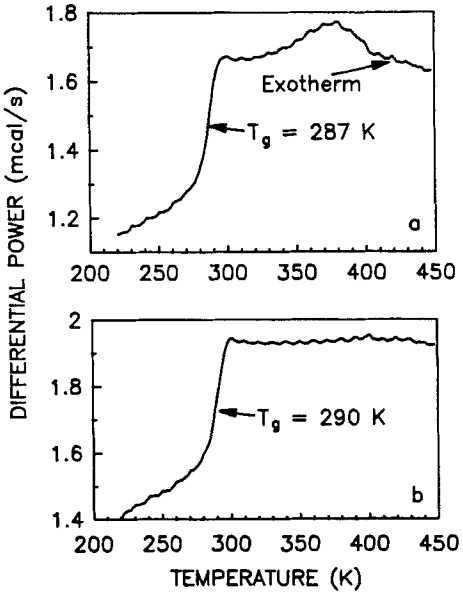

FIGURE 2 a) Initial DSC scan of NOA65A polymer matrix cured in e-beam apparatus. The change in baseline at about 287 K (14°C) is due to the glass transition temperature. The apparent peak at 380 K (107°C) is actually the leading edge of an exotherm due to post-curing of the polymer. b) Repeat scan of the sample of Figure 2a. The heat treatment resulting from the initial scan has increased the completeness of the cure, thus eliminating the exotherm previously observed. The glass transition temperature has increased by 3 K due to the enhanced degree of cure.

to that for ones cured by UV (see Figure 3), we can estimate the approximate cure temperature for the e-beam cured sample. The data of Figure 3 suggest that, for T_g = 290 K (17°C), the corresponding cure temperature is roughly 350 K (77°C). This result is in reasonable agreement with calculations of the temperature rise due to heating of the sample by the e-beam.

A.2 PDLC Film (ROTN404/NOA65A Sample). Figure 4a shows the initial DSC thermal scan for e-beam-cured sample No. 3 in Table I (i.e., the ROTN404:NOA65A = 1:1 system cured at 10Mrad.) Glass transitions are apparent at 224 K (−49°C) and at 265 K (−8°C). The one at the lower temperature is due to the multi-component liquid crystal in the microdroplets and is of no further interest for the present discussion; that at the higher temperature is the glass transition of the matrix material. A suggestion of a transition near 369 K (96°C) is somewhat masked by the onset of an exotherm at slightly higher temperature. However, the heat treatment produced during the scan of Figure 4a was sufficient to yield a more fully cured sample; this is clear from the subsequent scan (Figure 4b) in which the absence of the exotherm fully reveals the nematic-isotropic transition peak at 368 K (95°C). The slight (2°) increase in the matrix glass transition temperature reinforces the conclusion that the sample is more completely cured after the initial thermal scan. The magnitude of the matrix T_g for the ROTN404/

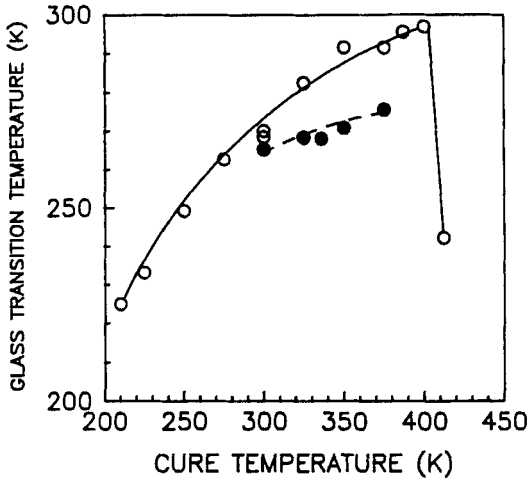

FIGURE 3 Glass transition temperature versus cure temperature for UV-cured samples of NOA65A (open circles) and ROTN404:NOA65A = 1:1 (filled circles). These results for UV-cured samples can be used to estimate the cure temperature for the e-beam cured systems of the present study. The T_g values for both the pure matrix and the PDLC film suggest a cure temperature of about 350 K (77°C) for the e-beam cured samples.

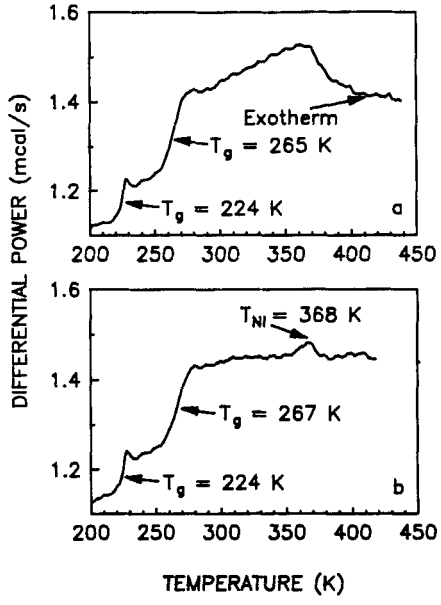

FIGURE 4 a) Initial DSC scan of ROTN404:NOA65A = 1:1 sample cured in e-beam apparatus with 10 Mrad dosage. The glass transition at about 224 K (−49°C) is due primarily to free liquid crystal in the microdroplets. However, liquid crystal at the surface or in cavities can also contribute. The glass transition at about 265 K (−8°C) is due to the polymer matrix, plasticized by the liquid crystal. An apparent transition at 369 K (96°C) is masked by the exotherm at higher temperature. b) Repeat of the scan of Figure 4a. The heat treatment resulting from the initial scan has increased the completeness of cure, eliminating the exotherm. The peak due to the nematic-isotropic transition at 368 K (95°C) is now clearly visible.

NOA65A sample is some 23° below that for the pure NOA65A matrix due to the plasticizing effect of the liquid crystal and is consistent with a cure temperature near 350 K (77°C).

From the magnitude of the nematic-isotropic transition enthalpy it is possible, using the methods of Reference 25, to estimate α, the fraction of liquid crystal contained in the microdroplets. Three different samples yielded ΔH_{NI} values ranging from 0.19 to 0.27 cal g^{-1}, corresponding to α values between 0.33 and 0.5. Thus, for these e-beam cured samples, as much as half to two-thirds of the liquid crystal is retained in the matrix. The reasons for the wide range and low values of α are uncertain. However, it may be that the rather short time available for the cure process (about 1 s) did not allow liquid crystal sufficient time to diffuse to droplet sites. Furthermore, the incompleteness of the cure resulted in sample-to-sample variations in microstructure, as was discovered with SEM. The values for α for the present system were somewhat lower than those for UV and thermally cured PDLC films, which generally range[25] from 0.6 to 0.9. Thus, it would appear that a number of improvements in the e-beam curing method are necessary before the technique can yield PDLC films with consistently good properties.

B. Film Microstructure

Using SEM we were able to determine the microstructure of the films. As shown in Table I, some of the samples exhibited the desired film morphology whereby the liquid crystal is confined to microdroplets dispersed in a continuous polymer matrix (see Figure 5a). However, many of the films exhibited a reverse morphology,[28,31] i.e., the continuum phase is the liquid crystal and the polymer material forms micro-balls which cluster together as illustrated in Figure 5b. The reasons for this different behavior were not established but may be similar to those proposed for the similar phase behavior observed in UV-cured PDLC films.[31]

The sample which exhibited best overall performance, sample No. 3 in Table I, exhibited a uniform droplet distribution with a mean droplet diameter in the 0.2–0.3 μm range. Figure 6 (double-hatched bars) shows the histogram of the diameters of the droplet cross sections seen on an electron microscope micrograph. Since these are the diameters of the *cross sections* of the droplets, not of the droplets themselves, we will call such a histogram a *planar histogram*.

From the planar histogram we will determine the true mean droplet diameter (that corresponding to the droplet volume distribution) and the total volume occupied by the droplets in the sample. We will also compare these values with those which can be estimated from the planar histogram.

A *true histogram* or volume histogram, that is, a histogram representing the distribution of the droplet diameters in the bulk of the sample, can be determined from the planar histogram as follows.[38–41] If the volume histogram is defined by a collection of n values N_i^V giving the number of droplet diameters found in unit volume of the sample with values between $(i-1)\Delta$ and $i\Delta$ where Δ is the bin size of the histogram, then the planar histogram corresponding to a cross sectional view of the sample is defined by an equal number of values N_i^A given by:

$$N_i^A = \Delta \sum_{j=0}^{n} a_{ij} N_j^V, \tag{3}$$

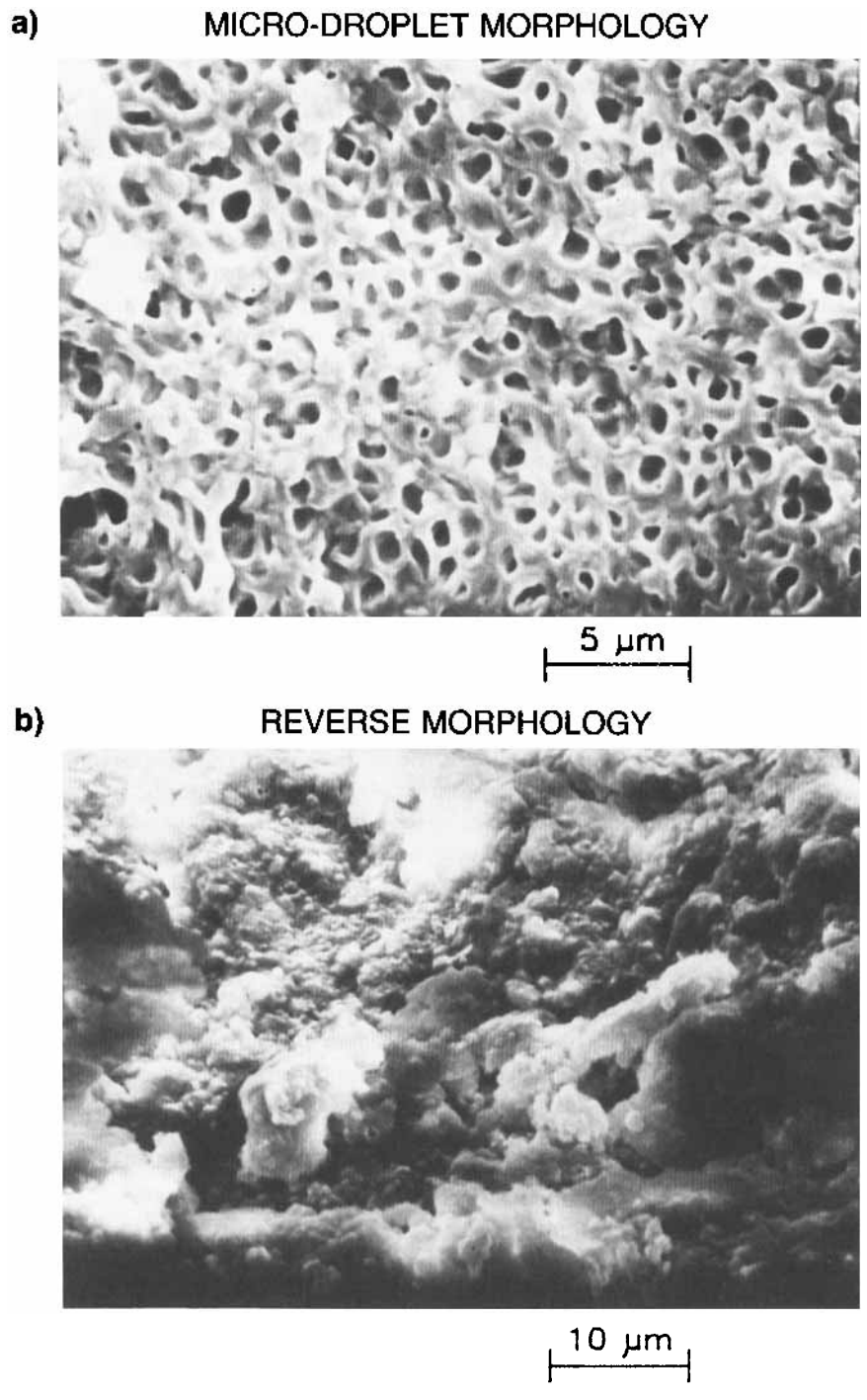

FIGURE 5 Scanning electron micrographs of cross-sections of e-beam cured samples illustrating: a) a microdroplet dispersion morphology corresponding to sample No. 3 in Table I, and b) a reverse morphology corresponding to sample No. 7 in Table I.

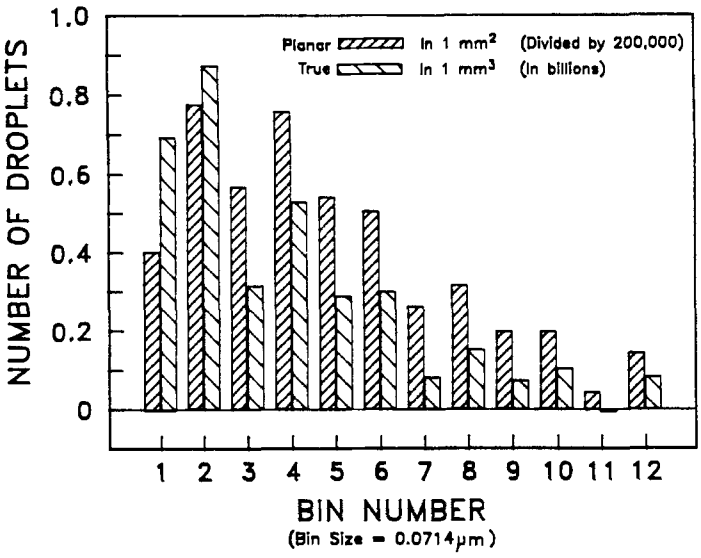

FIGURE 6 Histograms of the microdroplet-size distribution shown in Figure 5a. Double-hatched bars: planar histogram discribing the diameters of the droplet cross sections seen in the scanning electron micrograph; single-hatched bars: true or volume histogram describing the droplet diameters in the bulk of the sample (calculated from the planar histogram).

where

$$a_{ij} = \begin{cases} \sqrt{j^2 - (i-1)^2} - \sqrt{j^2 - i^2} & \text{if } i \leqslant j; \\ 0 & \text{if } i > i. \end{cases} \tag{4}$$

The inverse transformation, which expresses the N_i^V values of the true or volume histogram in terms of the N_j^A values of the planar histogram, is given by:

$$N_i^V = \Delta^{-1} \sum_{j=0}^{n} b_{ij} N_j^A, \tag{5}$$

where

$$b_{ij} = \begin{cases} -a_{ij}^{-1} \sum_{k=i}^{j-1} b_{ik} a_{kj} & \text{if } i < j; \\ a_{ii}^{-1} & \text{if } i = j; \\ 0 & \text{if } i > j. \end{cases} \tag{6}$$

Figure 6 (single-hatched bars) shows the true or volume histogram corresponding to the same sample. Notice that this histogram differs slightly from the planar histogram. Consequently, the mean droplet diameter $\overline{D}$ that can be calculated from the true histogram differs from that calculated from the planar histogram. For the

case under study we obtained $\overline{D} = 0.215$ μm from the true histogram and $\overline{D} = 0.277$ μm from the planar histogram. Although an expression relating these two mean values can be derived, such a discussion is beyond the scope of this work.

As mentioned above, the true volume fraction that the droplets occupy in the sample can be either estimated from the planar histogram or calculated exactly from the true histogram. The estimated value from the planar histogram is obtained assuming equipartition of the droplet volume fractions within each bin size and using the empirical fact that the volume fraction of the droplets should be equal to the area fraction of the cross sections of the droplets.[42] Under these assumptions we obtain a droplet volume fraction of 0.12. Using this value we can calculate the fraction of the initial liquid crystal which is confined in the droplets, α, to be $\alpha = 0.24$.

From the true histogram, however, we can obtain directly the volume fraction occupied by the droplets having to assume only equipartition of the droplet volume fractions within each bin size. We calculate from the true histogram a droplet volume fraction of 0.11, from which we calculate $\alpha = 0.22$. This value is very close to that obtained from the planar histogram, as expected, but is only in fair agreement with that estimated from the calorimetric measurements which give $\alpha = 0.33$ to 0.50 (see *A.2*). The fact that the histogram-calculated α-value is smaller than the DSC-derived α-value can be explained as follows.

First, the count of droplets in any given histogram will always be an underestimate because many droplets (especially the smaller ones) may not be clearly identifiable on the photograph, while there is no reason or mechanism to add droplets to the count. Second, DSC will most probably provide an overestimate because ΔH_{NI} will include not only a contribution from liquid crystal confined to the droplets but also from any free liquid crystal which may have migrated to the surface of the sample or become segregated into some larger cavity. Such cavities have been observed in UV-cured samples.

Finally, the true histogram may be analyzed to provide insight about the type of microdroplet size distribution. A random collection of objects is often well described by the logarithmic normal distribution function characterized by some mean value D_m and some distribution width[43] σ_g according to[44]:

$$p(D) = \frac{1}{(2\pi)^{1/2}\sigma_g D} \exp\left(\frac{-(\log D - \log D_m)^2}{2\sigma_g^2}\right). \tag{7}$$

This type of distribution differs from the usual normal or Gaussian distribution which cannot suitably represent a distribution of diameters because it admits negative values of D. In addition, unlike the normal distribution which is symmetrical, naturally occuring populations are frequently skewed. The logarithmic normal distribution satisfies these concerns and expresses that it is log D rather than D which is normally distributed.

One of the properties of the logarithmic normal distribution is that it generates a cumulative distribution function,

$$P(D) = \int_0^D p(D)dD, \tag{8}$$

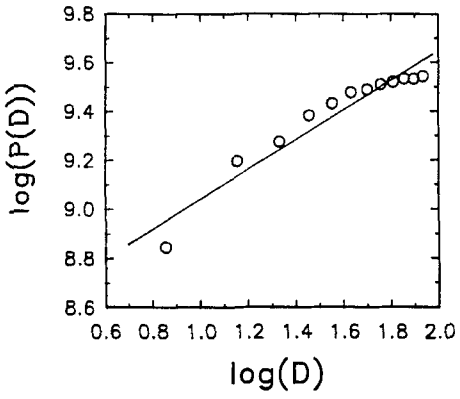

FIGURE 7 Plot of the logarithm of the cumulative distribution function of droplet sizes, obtained from the true droplet-size distribution shown in Figure 6, versus the logarithm of the droplet diameter (in nanometers). The straight line is a least squares fit to the data (circles).

whose logarithm is proportional to $\log(D)$. Thus, a plot of $\log(P(D))$ versus $\log D$ should yield a straight line for all object populations which are described by a logarithmic normal distribution.

Figure 7 shows the logarithm of the cumulative distribution values, which are obtained from the true or volume droplet-size distribution shown in Figure 6, plotted versus $\log D$, the logarithm of the droplet diameter at the center of each bin. The solid line is a least squares fit to the data (circles). The correlation of the straight line with the data is fair.

C. Sample Performance

As mentioned before, Table I is a summary of the results characterizing the performance of the different samples. We used four basic formulations differing in either the polymer matrix or the liquid crystal. Each of these formulations was studied at different e-beam dosages and, in one case, also at different liquid crystal/polymer volume ratios.

C.1 Film Thickness. We note (Table I) that the film thickness varied from sample to sample and was considerably larger than the spacers (17.5 μm). As mentioned before, in this preliminary work it was difficult to keep the two substrates pressed against each other while the sample passed under the e-beam. Future experiments will most certainly require improvements in this area.

C.2 Scattering Efficiency. The scattering efficiency of the various samples was determined by simple eye inspection and is shown in Table I as good (G) or as a failure to scatter light (F). Of the samples which failed to scatter light, sample 2 in Table I is of interest. This sample contained a relatively small volume fraction of liquid crystal. Since we have already shown from calorimetry and from SEM micrographs that a considerable amount of liquid crystal is retained in the polymer matrix, the fact that this sample failed to scatter light to an appreciable degree is

in accord with those previous observations. It suggests that only a small fraction of the liquid crystal in this sample aggregated into microdroplets.

C.3 Electro-Optic Response. Table I rates the samples in terms of their electro-optic response as good or poor. However, because of the large film thickness in most of the samples, it was difficult to electrically switch many of them. Since PDLC films, like other liquid crystal devices, are switched by the applied electric field rather than by the applied voltage, an increase in the film thickness results in an increase in the applied voltage necessary for its electro-optic activation. Thus, although some of the samples are stated to have poor electro-optic response, one should keep in mind that they might exhibit appropriate electro-optic response if they were thinner.

Figure 8 shows the spectral transmittance of sample No. 3 from 200 nm to 900 nm. These data were recorded using a Perkin-Elmer λ-5 spectrophotometer. The lower trace corresponds to the off-state ($V = 0$) and the upper trace to the on-state ($V = 100\ V_{rms}$ at 1 kHz). This e-beam-cured sample shows a very good electro-optic response, comparable to that obtained for similar, UV-cured PDLC films.[26–28]

Figure 9 shows the transmittance of the same sample as a function of applied voltage. It illustrates the fact that the threshold voltage, above which transmittance rises above 10%, is fairly large: 45 V_{rms} at 1 kHz. This high value may be a

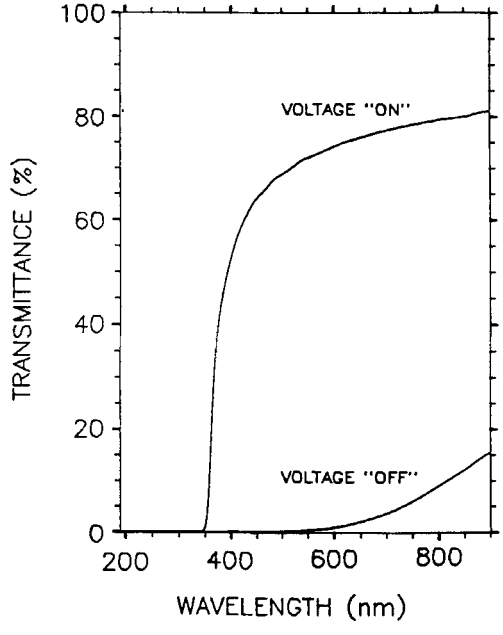

FIGURE 8 Transmittance versus wavelength for e-beam cured sample No. 3. The lower trace is for the non-switched off-state ($V = 0$) and the upper trace is for the switched on-state ($V = 100\ V_{rms}$ at 1 kHz).

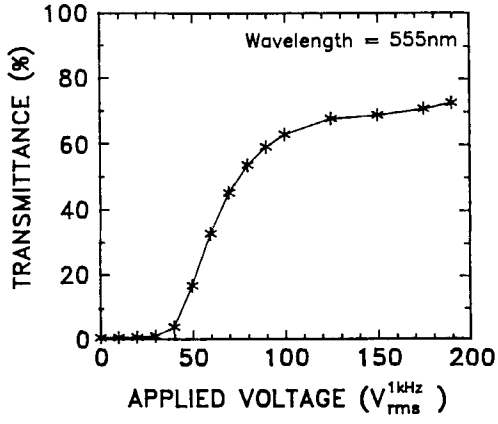

FIGURE 9 Transmittance versus applied voltage for e-beam cured sample No. 3.

consequence of the large film thickness (48 μm) which is substantially greater than the thickness of comparable UV-cured samples (18 μm) for which the threshold voltage is about 20 V_{rms}.[26] Similarly, the saturation voltage of the e-beam cured sample (150 V_{rms}) is also substantially greater than that measured in typical UV-cured samples[26-28] (60 V_{rms}).

Figure 10 shows the optical transmittance of sample No. 3 plotted versus temperature. These data were recorded using the same spectrophotometer referred to above. Two regions, below and above 90°C, may be distinguished in this figure.

Below about 90°C the transmittance in both the switched (upper trace) and non-switched (lower trace) states is typical of PDLC films.[26-28] The on-state is characterized by transmittance values near 60% over a wide temperature range. At low temperatures, below about 15°C, the electro-optic response is degraded as a

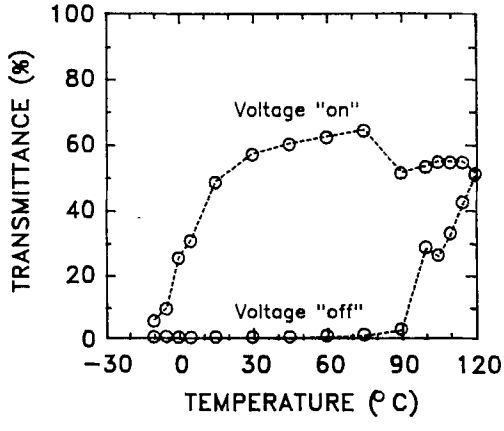

FIGURE 10 Transmittance versus temperature for e-beam cured sample No. 3. The lower trace is for the non-switched off-state (V = 0) and the upper trace is for the switched on-state (V = 100 V_{rms} at 1 kHz).

result of an increase in the elastic constants of the liquid crystal. Below $-10°C$ there is no detectable electro-optic response. Notice that this temperature is close to the glass transition of the polymer matrix, as determined from calorimetry (see *A.2*).

Above 90°C the electro-optic response is uncharacteristic of previously studied PDLC films.[26-28] Instead of detecting a collapse of the upper and lower traces into one single response curve, as expected if the liquid crystal were to undergo a phase transition from the liquid crystalline state to the isotropic state, we still observed on- and off- curves. These data were recorded on the first heating scan of the sample. Since our calorimetry results suggest that the polymer undergoes additional cross-linking during the initial heating (see *A.2*), we conclude that the unusual behavior of the transmittance data above 90°C is associated with post-curing effects. Unfortunately, subsequent heating runs of this sample could not be conducted: before all other data were completely analyzed, the sample was destroyed in SEM studies in order to determine its morphology.

We have also measured the response times of sample No. 3 by monitoring the transmittance as a sinusoidal voltage is gated on and off[26] (see Figure 11.) The rise time, 1.9 ms in response to an applied voltage of 120 V_{rms} at 4 kHz, and the decay time, 14.1 ms after turning off an applied voltage of 120 V_{rms} at 4 kHz, are slightly

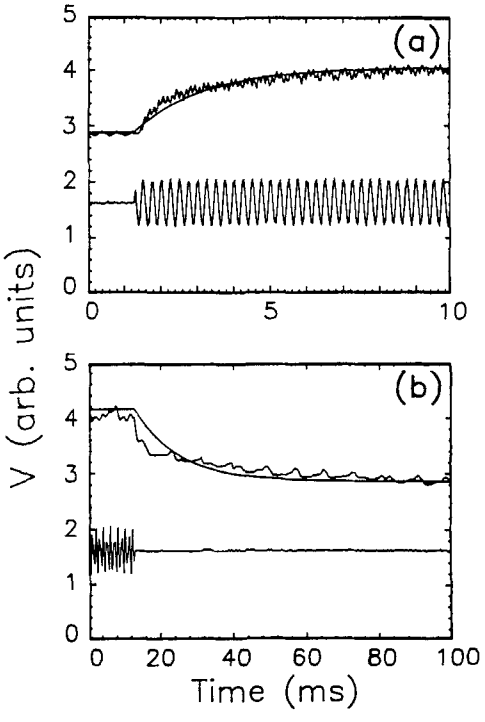

FIGURE 11 Response times of e-beam cured sample No. 3: a) rise time and b) decay time. The smooth curves are exponential fits to the transmittance data recorded as a sinusoidal applied voltage was turned on, (a), or off, (b). The driving voltage was 120 V_{rms} at 4 kHz.

shorter than those typically measured at room temperature for UV-cured samples,[26,27] typically 5 ms and 20 ms, respectively. Since the calorimetric measurements indicate that the sample might have not been fully cured, it is possible that the response times of PDLC films may be related to the degree of cure or rigidity of the polymer matrix.

C.4 Thermo-Optic Response. The thermo-optic response, i.e., the switching of a PDLC film from a scattering state to a transparent state at some temperature as the result of a phase transition of the liquid crystal from its liquid crystalline phase to its isotropic phase, was evaluated for all samples by visual inspection. As summarized in Table I, the results were good (G) for all samples except sample No. 6. Thus, even some of those samples which showed a reverse structural morphology exhibited good thermo-otpic response.

C.5 Sample Elongation. The elongation of the sample in response to an applied stress is of interest when the potential application of the PDLC film involves light polarization effects. As discovered gy Doane *et al*,[3] when a polymer dispersion of liquid crystal microdroplets is stretched along one direction, it partially polarizes light traveling through it so that the transmitted light is primarily polarized perpendicular to the direction of the applied stress. We tested for this behavior in the e-beam cured films. We observed that only the first series of films listed in Table I could be stretched enough to produce polarization effects. The other samples were nearly rigid or brittle. Since SEM micrographs of these samples reveal a reverse morphology microstructure, we ascribe their rigidity to a greater crosslinking of the polymer matrix.

C.6 Total Forward and Backscattered Powers. Finally, we measured the total transmitted and backscattered powers of sample No. 3 using an integrating sphere on a Perkin-Elmer λ-9 spectrophotometer.[27,45,46] The total solar-weighted transmitted power is 50% and the total solar-weighted reflected power is 37%. These values compare favorably with those measured for similar UV-cured samples.[27,45,46] Further improvements should be possible by modifying the cure conditions and sample formulation.

V. DISCUSSION AND CONCLUSIONS

A. e-Beam Cure Process

We have successfully demonstrated that PDLC films can be prepared using e-beam technology. The e-beam process was demonstrated to be feasible using both commercial formulations developed for UV-cure and special formulations which do not contain a photoinitiator. Thiol-enes, acrylates, and urethane-methacrylates all produced light scattering films. Although in some cases we observed a reverse morphology instead of the desirable droplet morphology, it is expected that, by proper selection of the cure conditions and the volume fraction of liquid crystal in the formulation, one should be able to readily prepare films with the correct morphology.

PET substrates were found to be suitable for the e-beam cure of PDLC films because no detectable discoloration was present after the radiation exposure. Most other substrates showed some discoloration, which may limit the applicability of the e-beam technique.

B. Degree of e-Beam Cure

Calorimetry has revealed that the e-beam-irradiated samples were incompletely cured but that heating to temperatures above 400 K (127°C) increased the degree of cure. Furthermore, the temperature of cure was roughly 350 K (77°C). The glass transition temperature of the PDLC film was about 23 degrees lower than that of the pure polymer matrix due to the plasticizing effect of the liquid crystal. The amount of liquid crystal contained in the microdroplets was smaller for the e-beam-cured samples than for thermally or UV-cured samples: 0.25–0.33 versus 0.6–0.9, respectively. The short duration of the cure process may be responsible for this result and also for the incompleteness of the cure. Therefore, if we are to benefit from the fast cure speeds of the e-beam technique, it will be necessary to improve the formulations in order to fully cure the polymer at desirable belt speeds.

C. Electro-Optic Response and Microstructure

The electro-optic response of e-beam cured films, measured in terms of transmittance versus wavelength, transmittance versus applied voltage, transmittance versus temperature, response times, and total solar-weighted forward and backscattered powers, is comparable to that of similar UV-cured films, thus showing promise for this cure technique.

True (i.e., volume) microdroplet-size histograms were calculated from the planar histograms obtained from cross-sections of the films observed with SEM. From such histograms we calculated the true mean droplet diameter. The mean droplet diameter computed from a planar histogram is somewhat larger than the mean value computed from the true or volume histogram: 0.277 versus 0.215 μm. The range of droplet sizes, from 0.05 to 1 μm, and the mean droplet diameter, 0.277 μm, which were obtained using the e-beam cure technique to prepare the PDLC films, are of the order of or smaller than the wavelength of visible light. This is desired in applications where the PDLC films are to strongly scatter visible light.

The volume fraction occupied by the droplets was also calculated. The volume fraction calculated from the planar histogram (0.12) is slightly larger than that calculated from the true histogram (0.11). From each of these values we calculated the fraction of initial liquid crystal which is confined in the droplets: $\alpha = 0.24$ and 0.22, respectively. Both values are in fair agreement with the range of values measured from DSC: from 0.33 to 0.5. Finally, we found that the droplet-size distribution is fairly well described by a logarithmic normal distribution function.

Acknowledgments

We thank Dan Hayden, Wilson Marion and Tom VanSteenkiste for valuable assistance in obtaining the data and Dave Lambert for helpful discussions. We thank Ted Tripp, Ken Hall and Denise Cleghorn from Energy Sciences for assistance during the e-beam cure experiments.

References

1. N. A. Vaz, G. W. Smith and G. P. Montgomery, Jr., *Mol. Cryst. Liq. Cryst.*, **146**, 17 (1987).
2. N. A. Vaz, G. W. Smith and G. P. Montgomery, Jr., *Mol. Cryst. Liq. Cryst.*, **146**, 1 (1987); N. A. Vaz and G. W. Smith, U.S. Patent 4,728,547, March 1, 1988.
3. J. W. Doane, N. A. Vaz, B.-G. Wu and S. Žumer, *Appl. Phys. Lett.*, **48**, 269 (1986).
4. J. W. Doane, G. Chidichimo and N. A. Vaz, U.S. Patent 4,688,900 (Aug. 25, 1987).
5. J. L. West, A. Golemme and J. W. Doane, U.S. Patent 4,763,255, June 16, 1987.
6. J. L. Fergason, U.S. Patents No. 4,435,047, March 6 (1984) and No. 4,616,903, October 14 (1986), and *SID Digest of Technical Papers*, **16**, 68 (1985).
7. P. S. Drzaic, *J. Appl. Phys.*, **60**, 2142 (1986), and *Mol. Cryst. Liq. Cryst.*, **154**, 289 (1988).
8. N. A. Vaz and G. P. Montgomery, Jr., *J. Appl. Phys.*, **62**, 3161 (1987).
9. J. L. West, *Mol. Cryst. Liq. Cryst.*, **157**, 427 (1988).
10. N. A. Vaz, G. W. Smith, T. H. VanSteenkiste and W. D. Marion, unpublished results.
11. A. M. Lackner, E. Ramos and J. D. Margerum, *Proc. SPIE*, **1080**, 267 (1989).
12. *Radiation Curing*, Edited by the Education Committee of the Radiation Curing Division, the Association for Finishing Processes of the Society of Manufacturing Engineers, Dearborn, Michigan, 1984.
13. Ted Tripp, Energy Sciences, private communication.
14. Norland Products, New Brunswick, NJ.
15. Aceto Chemical Co., Inc., Flushing, NY.
16. Diamond Shamrock, Morristown, NJ.
17. Polysciences Inc., Washington, PA.
18. EM Chemicals, Hawthorne, NY.
19. Hoffmann-La Roche, Nutley, NJ.
20. Donnelly Mirror, Inc., Holland, MI.
21. ITO coated borosilicate glass 140 μm thick, from Deposition Technology, Inc., San Diego, CA.
22. Sierracin Intrex, Sylmar, CA.
23. Glass fibers with nominal diameter 17.5 μm, from EM Chemicals, Hawthorne, NY.
24. Energy Sciences, Inc., Iwasaki, Japan. The machine used in our experiments is located at the Energy Sciences facility in Woburn, MA.
25. G. W. Smith and N. A. Vaz, *Liq. Cryst.*, **3**, 543 (1988).
26. G. P. Montgomery, Jr., N. A. Vaz and G. W. Smith, *Proc. SPIE*, **958**, 104 (1988).
27. G. P. Montgomery, *Proc. SPIE*, **1080**, 242 (1989).
28. N. A. Vaz, *Proc. SPIE*, **1080**, 2 (1989).
29. G. W. Smith, *Mol. Cryst. Liq. Cryst.*, **180B**, 201, 1990.
30. A. M. Lackner, J. D. Margerum, E. Ramos and K.-C. Lim, *Proc. SPIE*, **1080**, 53 (1989).
31. F. G. Yamagishi, L. J. Miller and C. I. van Ast, *Proc. SPIE*, **1080**, 24 (1989).
32. See Table I.
33. *CRC Handbook of Chemistry and Physics*, edited by the Chemical Rubber Co., 68th edition, CRC Press, Boca Raton, FL (1988).
34. G. W. Smith and N. A. Vaz, unpublished results.
35. K. Eiermann, *J. Pol. Sci., Polm. Symp. Ed.*, **6**, 157 (1964).
36. R. C. Steere, *J. Appl. Phys.*, **37**, 3338 (1966); *J. Appl. Phys.*, **38**, 3039 (1967); *J. Appl. Pol. Sci.*, **10**, 1673 (1966).
37. G. W. Smith, *Thermochim. Acta*, **112**, 289 (1987).
38. E. Scheil, *Z. Metallk.*, **27**, 199 (1935).
39. S. A. Saltykov, *Metals and Alloys*, **5**, 139 (1934).
40. R. T. DeHoff, *Trans. Metall. Soc. AIME*, **224**, 474 (1962).
41. J. R. Havens, D. B. Leong and K. B. Reimer, *Mol. Cryst. Liq. Cryst.*, **178**, 89 (1990).
42. This equality has been invoked by R. L. Fullman in *Trans. AIME, J. Metals*, **197**, 447 (1953) to derive relations between the average droplet diameter and other parameters characterizing the microstructure of materials observed in cross sections. We have independently arrived at this equality from computer models of the cross sections (N. A. Vaz, G. P. Montgomery, Jr. and R. E. Jacobsen, unpublished results).
43. σ_g is more properly called the geometric mean standard deviation.
44. A. Hald, *Statistical Theory with Engineering Applications*, Wiley, New York, 1955.
45. G. P. Montgomery, Jr., in *Large Area Chromogenics: Materials and Devices for Transmittance Control*, ed. by C. M. Lampert and C. G. Granqvist, SPIE Optical Engineering Press, WA, 1990.
46. N. A. Vaz and G. P. Montgomery, Jr., *J. Appl. Phys.*, **65**, 5043 (1989).